

## Exploring Competing Density Order in the Ionic Hubbard Model with Ultracold Fermions

Michael Messer,<sup>1</sup> Rémi Desbuquois,<sup>1</sup> Thomas Uehlinger,<sup>1</sup> Gregor Jotzu,<sup>1</sup> Sebastian Huber,<sup>2</sup> Daniel Greif,<sup>1</sup> and Tilman Esslinger<sup>1</sup>

<sup>1</sup>*Institute for Quantum Electronics, ETH Zurich, 8093 Zurich, Switzerland*

<sup>2</sup>*Institute for Theoretical Physics, ETH Zurich, 8093 Zurich, Switzerland*

(Received 18 March 2015; revised manuscript received 1 July 2015; published 9 September 2015)

We realize and study the ionic Hubbard model using an interacting two-component gas of fermionic atoms loaded into an optical lattice. The bipartite lattice has a honeycomb geometry with a staggered energy offset that explicitly breaks the inversion symmetry. Distinct density-ordered phases are identified using noise correlation measurements of the atomic momentum distribution. For weak interactions the geometry induces a charge density wave. For strong repulsive interactions we detect a strong suppression of doubly occupied sites, as expected for a Mott insulating state, and the externally broken inversion symmetry is not visible anymore in the density distribution. The local density distributions in different configurations are characterized by measuring the number of doubly occupied lattice sites as a function of interaction and energy offset. We further probe the excitations of the system using direction dependent modulation spectroscopy and discover a complex spectrum, which we compare with a theoretical model.

DOI: 10.1103/PhysRevLett.115.115303

PACS numbers: 67.85.Lm, 71.10.Fd, 71.30.+h, 73.22.Pr

Changes in the fundamental properties of interacting many-body systems are often determined by the competition between different energy scales, which may induce phase transitions. A particularly intriguing situation arises when the geometry of a system sets an energy scale that competes with the scale given by the interaction of its constituents. The importance of geometry is apparent in reduced dimensions which influences the interacting many-body system in its evolution from one phase to another [1]. A tractable approach to generic questions is provided by the ionic Hubbard model, which captures key aspects of the physics of a competing geometry and interactions in the charge sector. The Hamiltonian has a staggered energy offset on a bipartite lattice, such that the geometry supports a band insulating charge density wave (CDW). Conversely, strong repulsive on-site interactions favor a Mott insulating (MI) state at half-filling, which does not reflect the broken symmetry of the underlying lattice. The model was introduced in the context of charge-transfer organic salts [2,3] and has been proposed to explain strong electron correlations in ferroelectric perovskite materials [4]. Ultracold atoms in optical lattices are an excellent platform for studying competing energy scales, as they allow for tuning various parameters and the geometry of the Hamiltonian [5–17]. Here we explore the ionic Hubbard Model using ultracold fermions loaded into a tunable optical honeycomb potential.

The ionic Hubbard model has been studied theoretically in 1D chains [18–23] and on the 2D square lattice [24–27]. More recently, these studies have been extended to a honeycomb lattice, motivated by possible connections to superconductivity in layered nitrides [28] and strongly

correlated topological phases [29]. We consider the ionic Hubbard model on a honeycomb lattice:

$$\hat{H} = -t \sum_{\langle ij \rangle, \sigma} \hat{c}_{i\sigma}^\dagger \hat{c}_{j\sigma} + U \sum_i \hat{n}_{i\uparrow} \hat{n}_{i\downarrow} + \Delta \sum_{i \in \mathbf{A}, \sigma} \hat{n}_{i\sigma}, \quad (1)$$

where  $\hat{c}_{i\sigma}^\dagger$  and  $\hat{c}_{i\sigma}$  are the creation and annihilation operators of one fermion with spin  $\sigma = \uparrow, \downarrow$  on site  $i$  and  $\hat{n}_{i\sigma} = \hat{c}_{i\sigma}^\dagger \hat{c}_{i\sigma}$ . The system is characterized by three energies: the kinetic energy denoted by the tunneling amplitude  $t$  and summed over nearest neighbors  $\langle ij \rangle$ , the on-site interaction  $U$ , and the staggered energy offset between sites of the  $\mathbf{A}$  and  $\mathbf{B}$  sublattice  $\Delta$ , with  $\Delta > 0$ . In addition there is a harmonic confinement in all three directions. All parameters of the Hamiltonian are computed using Wannier functions [30].

The interplay between the interaction energy  $U$ , the energy offset  $\Delta$ , and tunneling  $t$  leads to quantum phases which differ by their density ordering. The two limiting cases can be qualitatively understood in the atomic limit at half-filling. For  $U \gg \Delta$  the system is described by a MI state. For a large energy offset  $\Delta \gg U$ , we expect a band insulator with staggered density and two fermions on lattice site  $\mathbf{B}$  [24]. The resulting CDW pattern reflects the broken inversion symmetry of the underlying geometry. We can characterize the transition by an order parameter  $N_{\mathbf{A}} - N_{\mathbf{B}}$ , which is zero in the MI state or when  $\Delta = 0$ , with  $N_{\mathbf{A}(\mathbf{B})}$  the total number of atoms on sublattice  $\mathbf{A}(\mathbf{B})$ . Figure 1(a) provides a schematic view of the different scenarios.

In order to realize the ionic Hubbard model we create a quantum degenerate cloud of  $^{40}\text{K}$  as described in previous work [30] and detailed in Ref. [31]. We prepare a balanced

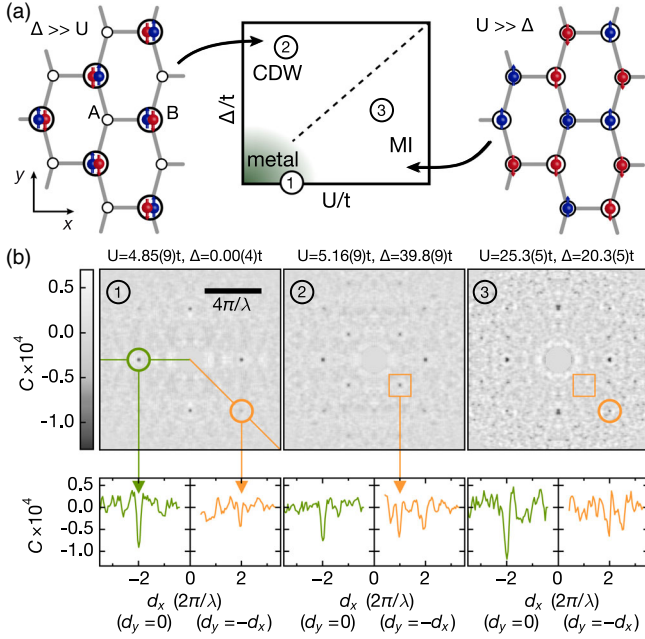


FIG. 1 (color online). Noise correlations. (a) Schematic view of the ionic Hubbard model on a honeycomb lattice at half-filling. Circles denote lattice sites **A** and **B**, where larger circles indicate lower potential energy. The phase diagram exhibits two limiting cases: For  $\Delta \gg U, t$  a CDW ordered state is expected with two fermions of opposite spin (red, blue) on lattice sites **B**, and empty sites **A**. In the other limit ( $U \gg \Delta, t$ ) a MI with one fermion on each lattice site should appear. (b) Measured noise correlation pictures obtained from absorption images of the atomic momentum distribution. Comparing panel 1 with panel 2, additional correlations appear due to broken inversion symmetry in the CDW ordered phase. When introducing strong interactions, these correlations are not observed anymore (panel 3), and the inversion symmetry of the density distribution no longer reflects the broken inversion symmetry of the lattice potential. Below each panel horizontal and diagonal cuts of the noise correlation image are shown. For the three different ratios of  $\Delta$  and  $U$ , between 165 and 201 measurements were taken each. We show the average of  $C(d_x, d_y)$  and  $C(d_x, -d_y)$ , which reflects the symmetry of the system.

fermionic spin mixture with total atom numbers between  $1.5 \times 10^5$  and  $2.0 \times 10^5$ , with 10% systematic uncertainty. A  $m_F = -9/2, -5/2$  [ $m_F = -9/2, -7/2$ ] mixture with temperatures of 16(2)% [13(2)%] of the Fermi temperature, is then loaded into a three-dimensional optical lattice within 200 ms. Using interfering laser beams at a wavelength  $\lambda = 1064$  nm we create a honeycomb potential in the  $xy$  plane, which is replicated along the  $z$  axis [14,30]. All tunneling bonds are set to  $t/h = 174(12)$  Hz. The tunable lattice allows us to independently adjust the energy offset  $\Delta = [0.00(4), 41(1)]t$  between the **A** and **B** sublattice [31]. Depending on the desired interaction strength we either use the Feshbach resonance of the  $m_F = -9/2, -7/2$  mixture or the  $m_F = -9/2, -5/2$  mixture.

We probe the spatial periodicity of the density distribution in the interacting many-body state by measuring correlations in the momentum distribution obtained after time-of-flight expansion and absorption imaging [32–37]. After preparing the system in a shallow honeycomb lattice with a given  $U$  and  $\Delta$ , we rapidly convert the lattice geometry to a deep simple cubic lattice. This ensures that we probe correlations of the underlying density order rather than a specific lattice structure. The atoms are released from the lattice and left to expand ballistically for 10 ms. We then measure the density distribution, which is proportional to the momentum distribution of the initial state  $n(\mathbf{q})$ . From this, we compute the correlator of the fluctuations of the momentum distribution [32–38],

$$C(\mathbf{d}) = \frac{\int \langle n(\mathbf{q}_0 - \mathbf{d}/2) \cdot n(\mathbf{q}_0 + \mathbf{d}/2) \rangle d\mathbf{q}_0}{\int \langle n(\mathbf{q}_0 - \mathbf{d}/2) \rangle \langle n(\mathbf{q}_0 + \mathbf{d}/2) \rangle d\mathbf{q}_0} - 1, \quad (2)$$

where the  $\langle \dots \rangle$  brackets denote the statistical averaging over absorption images taken under the same experimental conditions.

Owing to the fermionic nature of the particles, this quantity exhibits minima when  $\mathbf{d} = \mathbf{m}2\pi/\lambda$ , with  $\mathbf{m}$  a vector of integers [31]. This is illustrated by the anticorrelations of a repulsively interacting, metallic state with  $U = 4.85(9)t$  and  $\Delta = 0.00(4)t$ , shown in Fig. 1(b), left panel. There, the spatial periodicity of the atomic density follows the structure of the lattice potential, and minima in the correlator are observed for  $\mathbf{m} = (0, \pm 2)$  and  $\mathbf{m} = (\pm 2, 0)$ . For  $\Delta = 39.8(9)t$ , additional minima are observed at  $\mathbf{m} = (\pm 1, \pm 1)$ , see Fig. 1(b), central panel. For a simple cubic lattice potential of periodicity  $\lambda/2$ , the amplitude of these minima is given by [31]

$$C\left(\pm \frac{2\pi}{\lambda}, \pm \frac{2\pi}{\lambda}\right) \propto \frac{(N_{\mathbf{A}} - N_{\mathbf{B}})^2}{(N_{\mathbf{A}} + N_{\mathbf{B}})^2}. \quad (3)$$

Thus, the observation of additional minima confirms the presence of CDW ordering with  $N_{\mathbf{A}} \neq N_{\mathbf{B}}$ . Finally, for  $\Delta = 20.3(5)t$  and  $U = 25.3(5)t$ , these additional minima are not observed any more [see Fig. 1(b), right panel], signalling that with repulsive on-site interactions, the density distribution does not reflect the externally broken inversion symmetry. In this case the interactions suppress the CDW order, despite the presence of a large  $\Delta$ .

Based on these measurements we expect the local distribution of atoms on each lattice site to depend on the exact values of  $U$  and  $\Delta$ . We measure the fraction of atoms on doubly occupied sites  $D$  using interaction-dependent rf spectroscopy [8]. The number of doubly occupied sites compared to the number of singly occupied sites is directly related to the nature of the insulating states [39,40]: the MI state is signaled by a suppressed double occupancy while the CDW order is formed by atoms on alternating doubly occupied sites.

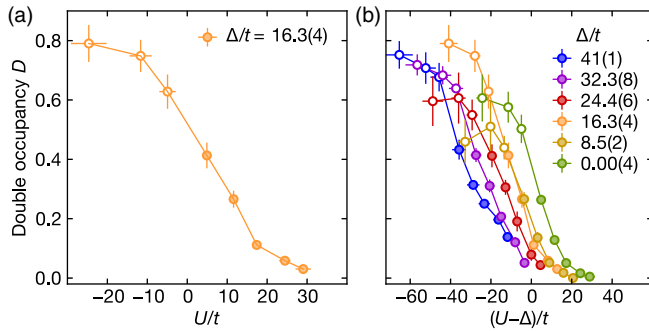


FIG. 2 (color online). Double occupancy measurement. (a) The measured double occupancy  $D$  as a function of the on-site interaction  $U$  for a fixed energy offset  $\Delta = 16.3(4)t$ . (b) For different values of  $\Delta$  (different colors) we obtain the double occupancy for a range of interactions  $U = [-24.6(13), 29.1(7)]t$ . Hollow (full) circles represent attractive (repulsive) interactions. Vertical error bars show the standard deviation of 5 measurements and horizontal error bars the uncertainty on our lattice parameters.

In the experiment we set an energy offset  $\Delta$  and measure  $D$  for different attractive and repulsive interactions  $U = [-24.6(13), +29.1(7)]t$ . Figure 2(a) shows  $D$  as a function of  $U$  at constant  $\Delta = 16.3(4)t$ . For strong attractive interactions we observe a large fraction of doubly occupied sites, which continuously decreases as  $U$  is increased. When tuning from attractive to weak repulsive interactions ( $\Delta \gg U$ ), we still observe a large  $D$  as expected for the CDW. For strong repulsive interactions ( $U \gg \Delta$ ) the measured double occupancy vanishes, the density pattern no longer reflects the broken inversion symmetry of the lattice, confirming the suppression of the CDW ordering. Figure 2(b) shows  $D$  as a function of the energy scale  $U - \Delta$ , which is the energy difference of a doubly occupied site neighboring an empty site compared to two singly occupied sites in the atomic limit. For the largest negative value of  $U - \Delta$  we observe the highest  $D$  for all  $\Delta$ . For positive values of  $U - \Delta$  the double occupancy continuously decreases and vanishes for the largest positive  $U - \Delta$ , consistent with a MI state. In contrast, for the intermediate regime the measured  $D$  depends on the individual values of  $U$  and  $\Delta$ , as now the finite temperature and chemical potential itself play an important role and a detailed analysis would be required for a quantitative understanding; however, we can qualitatively compare the dependence of  $D$  to an atomic limit calculation [31].

A characteristic feature of the MI and band insulating CDW state is a gapped excitation spectrum, which we probe using amplitude-modulation spectroscopy [8,41]. We sinusoidally modulate the intensity of the lattice beam in the  $y$  direction by  $\pm 10\%$  for 40 ms. Since the honeycomb lattice is created from several beams interfering in the  $xy$  plane [14], this leads to a modulation in tunnel coupling  $t_y$  of 20% and  $t_x$  of 8%, as well as a modulation of  $U$  by 4%

and  $\Delta$  by up to 6%. The interlayer tunneling  $t_z$  is not affected meaning that excitations only occur in the honeycomb plane. We set  $U = 24.4(5)t$  and measure  $D$  after the modulation for frequencies up to  $\nu = 11.6$  kHz ( $\approx 67t$ ). All measurements are performed in the quadratic-response regime [42].

Figure 3(a) shows the measured spectra for different values of  $\Delta$ . The MI state exhibits a gapped excitation spectrum, which is directly related to a particle-hole excitation with a gap of size  $U$  [8,30,42]. In the limit of  $\Delta = 0$  we detect this gap as a peak in the excitation spectrum at  $\nu = U/h$ . With increasing  $\Delta$  the single excitation peak splits into two peaks corresponding to different excitation energies [43]. The nature of the excitations can be understood as follows: The transfer of one particle costs approximately an energy of  $U - \Delta$  if a double occupancy is created on a **B** site and  $U + \Delta$  if it is created on an **A** site [see Fig. 3(b)]. The excitation of additional double occupancies shows that atoms were initially populating both sublattices, as expected in the MI regime. For small  $\Delta/U$  the system shows a clearly identifiable charge gap, which vanishes if  $U \sim \Delta$ . For large  $\Delta$  the charge gap reappears, and a minimum in the spectra reveals the breaking of double occupancies as a response to amplitude modulation. This is in agreement with the expected band insulating CDW, where double occupancies are on the **B** sublattice and **A** sites are empty.

The situation changes for amplitude modulation of the  $z$  lattice beam intensity by  $\pm 10\%$ . In this case excitations are created along links perpendicular to the honeycomb plane. Since the honeycomb lattice is replicated along the  $z$  axis, we observe a single peak at  $\nu = U/h$ , independent of the energy offset  $\Delta$  [see Fig. 3(c)]. The inset of Fig. 3(c) shows the direction dependent modulation spectrum for  $\Delta = 8.5(2)t$ , which allows us to independently determine the energy scales of the system in different spatial directions.

We extract the excitation energies by fitting multiple Gaussian curves to our experimental data and compare our results with the values of  $|U - \Delta|$ ,  $U + \Delta$  and  $U$  in Fig. 3(d). We observe a vanishing peak at  $U + \Delta$  for the largest  $\Delta$ . This is expected as there are fewer and fewer atoms on the **A** sublattice in the system for an increasing energy offset. Our measurements are in good agreement with a picture based on nearest-neighbor dynamics.

However, we observe additional peaks at  $\nu \approx U/h$  if  $U \sim \Delta$ , which cannot be understood in a two-site model. To rule out any higher-order contribution, we verified that the response signal has a quadratic dependence on the modulation parameters, as expected for a quadratic response [42]. This additional peak was also observed in a purely 2D ionic Hubbard model ( $t_z = h \times 2$  Hz), thus ruling out a contribution of excitations along the third direction [31].

To interpret the nature of the response at  $h\nu \approx U$  we calculate the kinetic energy response function

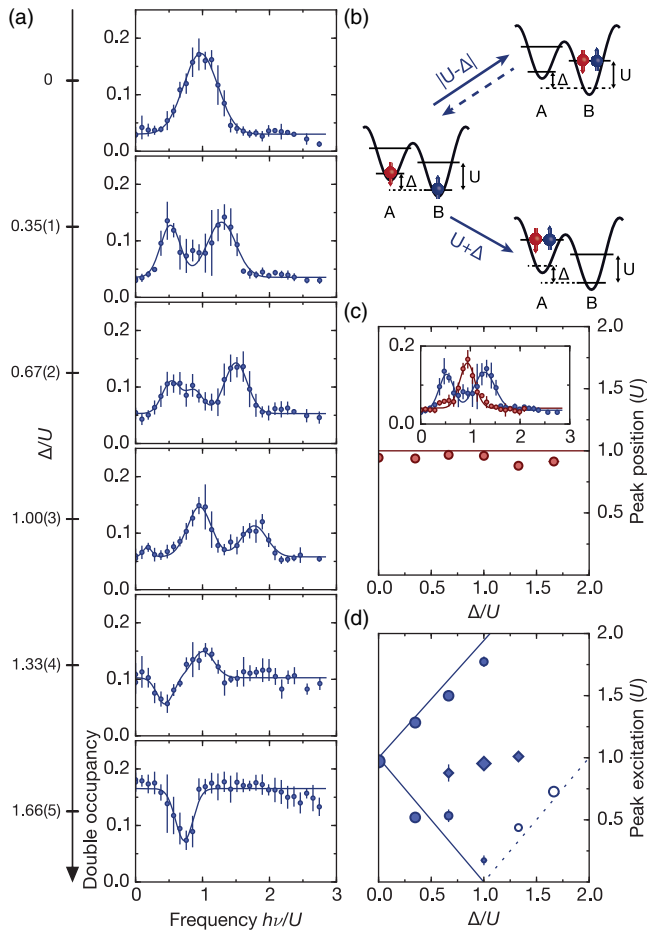


FIG. 3 (color online). Modulation spectroscopy measurement. (a) Excitation spectra observed by measuring the double occupancy  $D$  from amplitude modulation spectroscopy of the lattice beam in the  $y$  direction for different energy offsets  $\Delta$  at repulsive on-site interaction  $U = 24.4(5)t$ . Solid lines are multiple Gaussian fits to the modulation spectra. (b) Schematics for the relevant energy scales  $|U - \Delta|$  and  $U + \Delta$  as a response to the lattice modulation. (c) Modulation spectroscopy of the lattice beam in the  $z$  direction. The measured excitation frequencies are shown as a function of  $\Delta$  and compared to the value of  $U = 24.4(5)t$  (horizontal line). The inset shows the spatially dependent excitation spectrum. (d) Comparison of the measured excitation resonances (points) with the values of  $|U - \Delta|$ ,  $U + \Delta$  (lines). The area of the marker indicates the strength of the response (peak height) to the lattice modulation. Full (empty) circles represent a positive (negative) response in double occupancy. Error bars as in Fig. 2, vertical error bars in (c) and (d) show the fit error for the peak position.

$$\chi(\nu) = \sum_m \langle m | \delta D | m \rangle |\langle m | K | 0 \rangle|^2 \delta(h\nu - \epsilon_{m0}), \quad (4)$$

where the sum runs over all many-body states  $m$ ,  $\delta D = D - \langle 0 | D | 0 \rangle$  is the induced change in double occupancy,  $K = \sum_{\langle ij \rangle, \sigma} \hat{c}_{i\sigma}^\dagger \hat{c}_{j\sigma}$ , and  $\epsilon_{m0}$  denotes the excitation energy measured above the ground state  $|0\rangle$ . We evaluate  $\chi(\nu)$  in

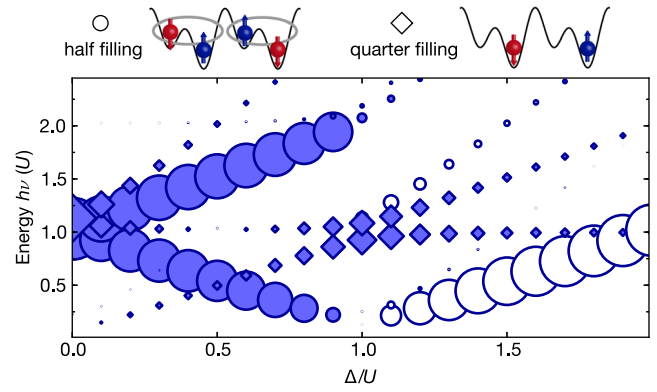


FIG. 4 (color online). Theoretical result for the kinetic energy response function  $\chi(\nu)$  of the double occupancy on a modulated four site model as a function of  $\Delta$  at constant  $U = 25t$ . Circular (diamond) data points represent the response for the half-filled (quarter-filled) case. The area of the marker shows the relative size of the calculated response, whereas full (empty) data points have a positive (negative) response signal.

exact diagonalization of a cluster of four sites for varying filling fractions.

The result shown in Fig. 4 for  $U/t = 25$  clearly indicates that the peak at  $h\nu \approx U$  around  $U = \Delta$  originates from regions of the lattice where the filling deviates from one particle per site [44]. In particular, for a configuration with two particles on four sites, the ground state at  $U = \Delta$  is a configuration with negligible double occupancy and only the lower sublattice sites are filled. The lattice modulation at  $h\nu \approx U$  then moves one particle to an energetically costly site. For  $U = \Delta$ , this configuration is resonantly coupled to a state where both particles are on the same, low-energy site. Hence, this process leads to an increase in the measured double occupancy. The analysis of such a four-site cluster qualitatively agrees with the observed signal at energy  $U$  in the intermediate ( $U \approx \Delta$ ) regime.

In conclusion, we have realized and studied the ionic Hubbard model with ultracold fermions in an optical honeycomb lattice. Our observations show that increasing interactions suppress the CDW order and restore inversion symmetry of the density distribution. Additionally, we probed correlations beyond nearest neighbor, which had not been accessible so far [45]. Future work can address open questions concerning the nature of the intermediate regime between the two insulating phases, which is theoretically debated and should depend on the dimensionality of the system [25,46]. Furthermore, we can extend our studies of the ionic Hubbard model to include topological phases by introducing complex next nearest-neighbor tunneling [29,47,48].

We thank Ulf Bissbort, Frederik Görg, Diana Prychynenko, Vijay Shenoy, Leticia Tarruell, Evert van Nieuwenburg, and Lei Wang for insightful discussions. We acknowledge funding from the SNF, NCCR-QSIT, QUIC (EU H2020-FETPROACT-2014) and SQMS (EU ERC

advanced grant). R. D. acknowledges support from ETH Zurich Postdoctoral Program and Marie Curie Actions for People COFUND program.

- 
- [1] T. Giamarchi, *Quantum Physics in One Dimension* (Oxford University Press, Oxford, 2003).
- [2] J. Hubbard and J. B. Torrance, *Phys. Rev. Lett.* **47**, 1750 (1981).
- [3] N. Nagaosa and J.-I. Takimoto, *J. Phys. Soc. Jpn.* **55**, 2735 (1986).
- [4] T. Egami, S. Ishihara, and M. Tachiki, *Science* **261**, 1307 (1993).
- [5] M. Lewenstein, A. Sanpera, and V. Ahufinger, *Ultracold Atoms in Optical Lattices: Simulating Quantum Many-Body Systems* (Oxford University Press, Oxford, 2012).
- [6] M. Greiner, O. Mandel, T. Esslinger, T. W. Hänsch, and I. Bloch, *Nature (London)* **415**, 39 (2002).
- [7] J. Sebby-Strabley, M. Anderlini, P. S. Jessen, and J. Porto, *Phys. Rev. A* **73**, 033605 (2006).
- [8] R. Jördens, N. Strohmaier, K. Günther, H. Moritz, and T. Esslinger, *Nature (London)* **455**, 204 (2008).
- [9] U. Schneider, L. Hackermüller, S. Will, T. Best, I. Bloch, T. A. Costi, R. W. Helmes, D. Rasch, and A. Rosch, *Science* **322**, 1520 (2008).
- [10] C. Sias, H. Lignier, Y. P. Singh, A. Zenesini, D. Ciampini, O. Morsch, and E. Arimondo, *Phys. Rev. Lett.* **100**, 040404 (2008).
- [11] R. Ma, M. E. Tai, P. M. Preiss, W. S. Bakr, J. Simon, and M. Greiner, *Phys. Rev. Lett.* **107**, 095301 (2011).
- [12] P. Soltan-Panahi, J. Struck, P. Hauke, A. Bick, W. Plenkers, G. Meineke, C. Becker, P. Windpassinger, M. Lewenstein, and K. Sengstock, *Nat. Phys.* **7**, 434 (2011).
- [13] J. Struck, C. Ölschläger, R. Le Targat, P. Soltan-Panahi, A. Eckardt, M. Lewenstein, P. Windpassinger, and K. Sengstock, *Science* **333**, 996 (2011).
- [14] L. Tarruell, D. Greif, T. Uehlinger, G. Jotzu, and T. Esslinger, *Nature (London)* **483**, 302 (2012).
- [15] F. Meinert, M. J. Mark, E. Kirilov, K. Lauber, P. Weinmann, A. J. Daley, and H.-C. Nägerl, *Phys. Rev. Lett.* **111**, 053003 (2013).
- [16] M. Di Liberto, T. Comparin, T. Kock, M. Ölschläger, A. Hemmerich, and C. Morais Smith, *Nat. Commun.* **5**, 5735 (2014).
- [17] S. Murmann, A. Bergschneider, V. M. Klinkhamer, G. Zürn, T. Lompe, and S. Jochim, *Phys. Rev. Lett.* **114**, 080402 (2015).
- [18] M. Fabrizio, A. O. Gogolin, and A. A. Nersisyan, *Phys. Rev. Lett.* **83**, 2014 (1999).
- [19] T. Wilkens and R. M. Martin, *Phys. Rev. B* **63**, 235108 (2001).
- [20] A. Kampf, M. Sekania, F. Hébert, and P. Brune, *J. Phys. Condens. Matter* **15**, 5895 (2003).
- [21] S. R. Manmana, V. Meden, R. M. Noack, and K. Schönhammer, *Phys. Rev. B* **70**, 155115 (2004).
- [22] C. D. Batista and A. A. Aligia, *Phys. Rev. Lett.* **92**, 246405 (2004).
- [23] M. E. Torio, A. A. Aligia, G. I. Japaridze, and B. Normand, *Phys. Rev. B* **73**, 115109 (2006).
- [24] S. S. Kancharla and E. Dagotto, *Phys. Rev. Lett.* **98**, 016402 (2007).
- [25] N. Paris, K. Bouadim, F. Hebert, G. G. Batrouni, and R. T. Scalettar, *Phys. Rev. Lett.* **98**, 046403 (2007).
- [26] K. Bouadim, N. Paris, F. Hébert, G. G. Batrouni, and R. T. Scalettar, *Phys. Rev. B* **76**, 085112 (2007).
- [27] A. T. Hoang, *J. Phys. Condens. Matter* **22**, 095602 (2010).
- [28] T. Watanabe and S. Ishihara, *J. Phys. Soc. Jpn.* **82**, 034704 (2013).
- [29] D. Prychynenko and S. D. Huber, arXiv:1410.2001.
- [30] T. Uehlinger, G. Jotzu, M. Messer, D. Greif, W. Hofstetter, U. Bissbort, and T. Esslinger, *Phys. Rev. Lett.* **111**, 185307 (2013).
- [31] See Supplemental Material at <http://link.aps.org/supplemental/10.1103/PhysRevLett.115.115303> for details.
- [32] E. Altman, E. Demler, and M. D. Lukin, *Phys. Rev. A* **70**, 013603 (2004).
- [33] S. Fölling, F. Gerbier, A. Widera, O. Mandel, T. Gericke, and I. Bloch, *Nature (London)* **434**, 481 (2005).
- [34] T. Rom, T. Best, D. van Oosten, U. Schneider, S. Fölling, B. Paredes, and I. Bloch, *Nature (London)* **444**, 733 (2006).
- [35] I. B. Spielman, W. D. Phillips, and J. V. Porto, *Phys. Rev. Lett.* **98**, 080404 (2007).
- [36] V. Guarrera, N. Fabbri, L. Fallani, C. Fort, K. M. R. van der Stam, and M. Inguscio, *Phys. Rev. Lett.* **100**, 250403 (2008).
- [37] J. Simon, W. S. Bakr, R. Ma, M. E. Tai, P. M. Preiss, and M. Greiner, *Nature (London)* **472**, 307 (2011).
- [38] See Supplemental Material at <http://link.aps.org/supplemental/10.1103/PhysRevLett.115.115303> for details on the data processing required to compute this quantity and the detection protocol of the noise correlations.
- [39] V. W. Scarola, L. Pollet, J. Oitmaa, and M. Troyer, *Phys. Rev. Lett.* **102**, 135302 (2009).
- [40] L. De Leo, J.-S. Bernier, C. Kollath, A. Georges, and V. W. Scarola, *Phys. Rev. A* **83**, 023606 (2011).
- [41] C. Kollath, A. Iucci, I. P. McCulloch, and T. Giamarchi, *Phys. Rev. A* **74**, 041604 (2006).
- [42] D. Greif, L. Tarruell, T. Uehlinger, R. Jördens, and T. Esslinger, *Phys. Rev. Lett.* **106**, 145302 (2011).
- [43] Related excitations have been observed with bosons in tilted optical lattices [10,11,15] and for two fermions in a double-well potential [17].
- [44] Because of the harmonic confinement our system exhibits a large fraction of atoms away from half-filling, for more details see Supplemental Material at <http://link.aps.org/supplemental/10.1103/PhysRevLett.115.115303>.
- [45] D. Greif, T. Uehlinger, G. Jotzu, L. Tarruell, and T. Esslinger, *Science* **340**, 1307 (2013).
- [46] A. Garg, H. R. Krishnamurthy, and M. Randeria, *Phys. Rev. Lett.* **97**, 046403 (2006).
- [47] G. Jotzu, M. Messer, R. Desbuquois, M. Lebrat, T. Uehlinger, D. Greif, and T. Esslinger, *Nature (London)* **515**, 237 (2014).
- [48] W. Zheng, H. Shen, Z. Wang, and H. Zhai, *Phys. Rev. B* **91**, 161107 (2015).